

Low-Rank Tensor Completion Based on Bivariate Equivalent Minimax-Concave Penalty

Hongbing Zhang, Xinyi Liu, Hongtao Fan, Yajing Li, Yinlin Ye .

Abstract—Low-rank tensor completion (LRTC) is an important problem in computer vision and machine learning. The minimax-concave penalty (MCP) function as a non-convex relaxation has achieved good results in the LRTC problem. To make all the constant parameters of the MCP function as variables so that further improving the adaptability to the change of singular values in the LRTC problem, we propose the bivariate equivalent minimax-concave penalty (BEMCP) theorem. Applying the BEMCP theorem to tensor singular values leads to the bivariate equivalent weighted tensor Γ -norm (BEWTGN) theorem, and we analyze and discuss its corresponding properties. Besides, to facilitate the solution of the LRTC problem, we give the proximal operators of the BEMCP theorem and BEWTGN. Meanwhile, we propose a BEMCP model for the LRTC problem, which is optimally solved based on alternating direction multiplier (ADMM). Finally, the proposed method is applied to the data restorations of multispectral image (MSI), magnetic resonance imaging (MRI) and color video (CV) in real-world, and the experimental results demonstrate that it outperforms the state-of-arts methods.

Index Terms—Bivariate equivalent minimax-concave penalty (BEMCP), bivariate equivalent weighted tensor Γ -norm (BEWTGN), low-rank tensor completion (LRTC).

I. INTRODUCTION

WITH the rapid development of information technology, researchers increasingly encounter real data with high dimensions and complex structures. Tensors, as high-dimensional generalizations of vectors and matrices, can better represent the complex properties of high-dimensional data and play an increasingly important role in many applications, such as color image/video (CI/CV) processing [1], [2], [3], [4], hyperspectral/multispectral image (HSI/MSI) processing [5], [6], [7], [8], magnetic resonance imaging (MRI) data recovery [9], [10], [11], background subtraction [12], [13], [14], video rain stripe removal [15], [16] and signal reconstruction [17], [18].

Low-rank tensor completion (LRTC) is an important issue in tensor recovery research. The general method expresses the low-rank tensor completion problem as follows:

$$\min_X \text{rank}(X) \quad \text{s.t.} \quad \mathcal{P}_\Omega(X - \mathcal{Y}) = \mathbf{0}, \quad (1)$$

This work was supported by the National Natural Science Foundation of China (Nos. 11701456, 11801452, 11571004), Fundamental Research Project of Natural Science in Shaanxi Province General Project (Youth) (Nos. 2019JQ-415, 2019JQ-196), the Initial Foundation for Scientific Research of Northwest A&F University (Nos.2452017219, 2452018017), and Innovation and Entrepreneurship Training Program for College Students of Shaanxi Province (S201910712132).

H. Zhang, X. Liu, H. Fan, Y. Li and Y. Ye are with Department of information and Computing Science, College of Science, Northwest A&F University, Yangling, Shaanxi 712100, China (e-mail: zhanghb@nwfufu.edu.cn; Lxy6x1@163.com; fanht17@nwfufu.edu.cn; hliyajing@163.com; 13314910376@163.com)

where $\mathcal{Y} \in \mathbb{R}^{I_1 \times I_2 \times \dots \times I_N}$ is the observation, Ω is the index set for the known entries, and $\mathcal{P}_\Omega(\mathcal{Y})$ is a projection operator that keeps the entries of \mathcal{Y} in Ω and sets all others to zero, $\text{rank}(X)$ defines the tensor rank of X . In fact, tensors differ from matrices in that the definition of their rank is not unique. In the past decades, the most popular definitions of rank are CANDECOMP/PARAFAC (CP) rank based on CP decomposition [19], [20] and Tucker rank based on Tucker decomposition [21], [22], as well as tubal rank and multi-rank based on t-SVD [23]. Solving the CP rank problem of tensors is a NP-hard [24], which is not conducive to better application. The calculation of Tucker rank requires data to be folded and unfolded, which will cause structural damage to data. Compared with CP rank and Tucker rank, the tubal rank and multiple rank obtained based on t-SVD can better maintain the data structure, but its tensor-tensor product limitation prevents it from being applied to higher order cases. Recently, Zheng et al. [25] proposed a new form of rank (N-tubal rank) based on tubal rank, which adopts a new unfold method of higher-order tensors into third-order tensors in various directions. This approach makes good use of the properties of tensor tubal rank but also enables t-SVD to be applied to higher-order cases. Therefore, because of the excellent properties of N-tubal rank, we will also consider N-tubal rank to construct the model we propose in this paper.

Undoubtedly, the development of computationally efficient algorithms to solve problem (1) is of great practical value. However, the rank optimization problem in problem (1) will lead to NP-hard problem [24], which will seriously affect the efficiency of solving the problem. In this regard, researchers turn to its convex relaxation or non-convex relaxation forms. For convex relaxation, although it is easier to solve, it will produce biased estimates [26]. It is relatively difficult to solve for non-convex relaxations, but leads to more accurate results [27], [28], [29]. Recently, the minimax-concave penalty function as a non-convex relaxation has achieved good results in the LRTC problem [30], [31]. Further research on this function has profound implications for the LRTC problem, and its definition is as follows:

Definition 1 (Minimax-concave penalty (MCP) function [32]): Let $\lambda > 0, \gamma > 1$. The minimax-concave penalty function $h_{\gamma, \lambda} : \mathbb{R} \rightarrow \mathbb{R}_{\geq 0}$ is defined as

$$h_{\gamma, \lambda}(y) = \begin{cases} \lambda|y| - \frac{y^2}{2\gamma}, & |y| \leq \gamma\lambda, \\ \frac{\lambda^2}{2\gamma}, & |y| \geq \gamma\lambda. \end{cases} \quad (2)$$

It is not difficult to find that the MCP function contains two constant parameters, i.e., λ and γ . It is considered that

in the LRTC problem when the MCP function acts on the tensor singular values, its parameters are fixed. But the tensor singular values will change with the iteration update. Recently, an equivalent MCP (EMCP) method was proposed in [33], which is a novel non-convex relaxation method based on the traditional MCP method. The EMCP transforms the parameter λ in MCP into a variable form through the equivalence theorem so that it can adapt to the change of tensor singular values. It is worth noting that the MCP function contains two parameters, i.e., λ and γ , which, in reality, affect each other, and the nonconvex relaxations produced by different λ and γ vary widely. A key idea is that it is especially important to expect to turn both parameters into variables at the same time, resulting in a more efficient equivalence theorem. Motivated by this, we propose a new structural equivalence theorem, i.e., the bivariate equivalent minimax-concave penalty (BEMCP) theorem, that allows λ and γ to be transformed into variables at the same time. The difference between MCP, EMCP, and BEMCP can be seen from the Table I.

TABLE I
VARIABLE CASE FOR THREE METHODS

Method	Variable	
	λ	γ
MCP	×	×
EMCP	√	×
BEMCP	√	√

The symbols "√" and "×" indicate whether λ and γ are variables or not.

To sum up, the main contributions of our paper are:

Firstly, a new structural equivalence theorem called BEMCP theorem is proposed, which turns two constant parameters λ and γ into variables at the same time and further improves adaptability of tensor singular value change in the LRTC problem. Applying the BEMCP theorem to tensor singular values leads to the bivariate equivalent weighted tensor Γ -norm (BEWTGN) theorem, and the corresponding properties are analyzed and discussed. Furthermore, to solve the established model based on this new theorem, the corresponding proximal operators of the BEMCP theorem and BEWTGN are proposed.

Secondly, for the LRTC problem, we propose a new model, i.e., BEMCP model based on N-tubal rank. Furthermore, we design an efficient alternating direction multiplier method (ADMM) algorithm [34], [35] to optimally solve these problems. On this basis, the closed solution of each variable update is deduced, so that the algorithm can be executed efficiently.

Thirdly, three different types of data, i.e., MSI, MRI, and CV, are used to verify the effectiveness and efficiency of proposed method. Extensive numerical experiments demonstrate that the results obtained by our method have clear advantages over the comparative method in both visual and quantitative values.

The summary of this article is as follows: In Section II, some preliminary knowledge and background of the tensors are given. The theorems about BEMCP and its properties are

presented in Section III. In Section IV, we give the corresponding proximal operators and proofs of the BEMCP theorem and BEWTGN. The main results, including the proposed model and algorithm, are shown in Section V. The results of extensive experiments and discussions are presented in Section VI. Conclusions are drawn in Section VII.

II. PRELIMINARIES

A. Tensor Notations and Definitions

In this section, we give some basic notations and briefly introduce some definitions used throughout the paper. Generally, a lowercase letter and an uppercase letter denote a vector y and a matrix Y , respectively. An N -th-order tensor is denoted by a calligraphic uppercase letter $\mathcal{Y} \in \mathbb{R}^{I_1 \times I_2 \times \dots \times I_N}$ and $\mathcal{Y}_{i_1, i_2, \dots, i_N}$ is its (i_1, i_2, \dots, i_N) -th element. The Frobenius norm of a tensor is defined as $\|\mathcal{Y}\|_F = (\sum_{i_1, i_2, \dots, i_N} y_{i_1, i_2, \dots, i_N}^2)^{1/2}$. For a three order tensor $\mathcal{Y} \in \mathbb{R}^{I_1 \times I_2 \times I_3}$, we use $\bar{\mathcal{Y}}$ to denote along each tubal of \mathcal{Y} , i.e., $\bar{\mathcal{Y}} = \text{fft}(\mathcal{Y}, [], 3)$. The inverse DFT is computed by command ifft satisfying $\mathcal{Y} = \text{ifft}(\bar{\mathcal{Y}}, [], 3)$. More often, the frontal slice $\mathcal{Y}(:, :, i)$ is denoted compactly as $\mathcal{Y}^{(i)}$. The Hadamard product is the elementwise tensor product. Given tensors \mathcal{A} and \mathcal{B} , both of size $I_1 \times I_2 \times \dots \times I_N$, their Hadamard product is denoted by $\mathcal{A} \star \mathcal{B}$. And the elementwise tensor division is denoted by $\frac{\mathcal{A}}{\mathcal{B}}$. The set of real numbers greater than b real numbers is denoted as $\mathbb{R}_{\geq b} = \{v \in \mathbb{R} \mid v \geq b\}$. The set of tensors consisting of all real-valued elements greater than b can be expressed as $\mathbb{R}_{\geq b}^{I_1 \times I_2 \times \dots \times I_N} = \{\bar{v} \in \mathbb{R}^{I_1 \times I_2 \times \dots \times I_N} \mid \bar{v}_{i_1, i_2, \dots, i_N} \geq b\}$.

Definition 2 (Mode- $k_1 k_2$ slices [25]): For an N -th-order tensor $\mathcal{Y} \in \mathbb{R}^{I_1 \times I_2 \times \dots \times I_N}$, its mode- $k_1 k_2$ slices ($\mathcal{Y}^{(k_1 k_2)}, 1 \leq k_1 < k_2 \leq N, k_1, k_2 \in \mathbb{Z}$) are two-dimensional sections, defined by fixing all but the mode- k_1 and the mode- k_2 indexes.

Definition 3 (Tensor Mode- k_1, k_2 Unfolding and Folding [25]): For an N -th-order tensor $\mathcal{Y} \in \mathbb{R}^{I_1 \times I_2 \times \dots \times I_N}$, its mode- $k_1 k_2$ unfolding is a three order tensor denoted by $\mathcal{Y}_{(k_1 k_2)} \in \mathbb{R}^{I_{k_1} \times I_{k_2} \times \prod_{s \neq k_1, k_2} I_s}$, the frontal slices of which are the lexicographic orderings of the mode- $k_1 k_2$ slices of \mathcal{Y} . Mathematically, the (i_1, i_2, \dots, i_N) -th element of \mathcal{Y} maps to the (i_{k_1}, i_{k_2}, j) -th element of $\mathcal{Y}_{(k_1 k_2)}$, where

$$j = 1 + \sum_{s=1, s \neq k_1, s \neq k_2}^N (i_s - 1)J_s \quad \text{with} \quad J_s = \prod_{m=1, m \neq k_1, m \neq k_2}^{s-1} I_m. \quad (3)$$

The mode- $k_1 k_2$ unfolding operator and its inverse operation are respectively represented as $\mathcal{Y}_{(k_1 k_2)} := t\text{-unfold}(\mathcal{Y}, k_1, k_2)$ and $\mathcal{Y} := t\text{-fold}(\mathcal{Y}_{(k_1 k_2)}, k_1, k_2)$.

For a three order tensor $\mathcal{Y} \in \mathbb{R}^{I_1 \times I_2 \times I_3}$, the block circulation operation is defined as

$$\text{bcirc}(\mathcal{Y}) := \begin{pmatrix} \mathcal{Y}^{(1)} & \mathcal{Y}^{(I_3)} & \dots & \mathcal{Y}^{(2)} \\ \mathcal{Y}^{(2)} & \mathcal{Y}^{(1)} & \dots & \mathcal{Y}^{(3)} \\ \vdots & \vdots & \ddots & \vdots \\ \mathcal{Y}^{(I_3)} & \mathcal{Y}^{(I_3-1)} & \dots & \mathcal{Y}^{(1)} \end{pmatrix} \in \mathbb{R}^{I_{I_3} \times I_2 \times I_3}.$$

The block diagonalization operation and its inverse operation are given by

$$bdiag(\mathcal{Y}) := \begin{pmatrix} \mathcal{Y}^{(1)} & & & \\ & \mathcal{Y}^{(2)} & & \\ & & \ddots & \\ & & & \mathcal{Y}^{(I_3)} \end{pmatrix} \in \mathbb{R}^{I_1 I_3 \times I_2 I_3},$$

$$bdfold(bdiag(\mathcal{Y})) := \mathcal{Y}.$$

The block vectorization operation and its inverse operation are defined as

$$bvec(\mathcal{Y}) := \begin{pmatrix} \mathcal{Y}^{(1)} \\ \mathcal{Y}^{(2)} \\ \vdots \\ \mathcal{Y}^{(I_3)} \end{pmatrix} \in \mathbb{R}^{I_1 I_3 \times I_2}, \quad bvfold(bvec(\mathcal{Y})) := \mathcal{Y}.$$

Definition 4 (T-product [36]): Let $\mathcal{A} \in \mathbb{R}^{I_1 \times I_2 \times I_3}$ and $\mathcal{B} \in \mathbb{R}^{I_2 \times J \times I_3}$. Then the t-product $\mathcal{A} * \mathcal{B}$ is defined to be a tensor of size $I_1 \times J \times I_3$,

$$\mathcal{A} * \mathcal{B} := bvfold(bcirc(\mathcal{A})bvec(\mathcal{B})).$$

Since that circular convolution in the spatial domain is equivalent to multiplication in the Fourier domain, the T-product between two tensors $\mathcal{C} = \mathcal{A} * \mathcal{B}$ is equivalent to

$$\tilde{\mathcal{C}} = bdfold(bdiag(\tilde{\mathcal{A}})bdiag(\tilde{\mathcal{B}})).$$

Definition 5 (Tensor conjugate transpose [36]): The conjugate transpose of a tensor $\mathcal{A} \in \mathbb{C}^{I_1 \times I_2 \times I_3}$ is the tensor $\mathcal{A}^H \in \mathbb{C}^{I_2 \times I_1 \times I_3}$ obtained by conjugate transposing each of the frontal slices and then reversing the order of transposed frontal slices 2 through I_3 .

Definition 6 (Identity tensor [36]): The identity tensor $\mathcal{I} \in \mathbb{R}^{I_1 \times I_1 \times I_3}$ is the tensor whose first frontal slice is the $I_1 \times I_1$ identity matrix, and whose other frontal slices are all zeros.

It is clear that $bcirc(\mathcal{I})$ is the $I_1 I_3 \times I_1 I_3$ identity matrix. So it is easy to get $\mathcal{A} * \mathcal{I} = \mathcal{A}$ and $\mathcal{I} * \mathcal{A} = \mathcal{A}$.

Definition 7 (Orthogonal tensor [36]): A tensor $\mathcal{Q} \in \mathbb{R}^{I_1 \times I_1 \times I_3}$ is orthogonal if it satisfies

$$\mathcal{Q} * \mathcal{Q}^H = \mathcal{Q}^H * \mathcal{Q} = \mathcal{I}.$$

Definition 8 (F-diagonal tensor [36]): A tensor is called f-diagonal if each of its frontal slices is a diagonal matrix.

Theorem 1 (t-SVD [37]): Let $\mathcal{X} \in \mathbb{R}^{I_1 \times I_2 \times I_3}$ be a three order tensor, then it can be factored as

$$\mathcal{X} = \mathcal{U} * \mathcal{S} * \mathcal{V}^H,$$

where $\mathcal{U} \in \mathbb{R}^{I_1 \times I_1 \times I_3}$ and $\mathcal{V} \in \mathbb{R}^{I_2 \times I_2 \times I_3}$ are orthogonal tensors, and $\mathcal{S} \in \mathbb{R}^{I_1 \times I_2 \times I_3}$ is an f-diagonal tensor.

Definition 9 (Tensor tubal-rank and multi-rank [23]): The tubal-rank of a tensor $\mathcal{Y} \in \mathbb{R}^{I_1 \times I_2 \times I_3}$, denoted as $rank_t(\mathcal{Y})$, is defined to be the number of non-zero singular tubes of \mathcal{S} , where \mathcal{S} comes from the t-SVD of \mathcal{Y} : $\mathcal{Y} = \mathcal{U} * \mathcal{S} * \mathcal{V}^H$. That is

$$rank_t(\mathcal{Y}) = \#\{i : \mathcal{S}(i, :, :) \neq 0\}. \quad (4)$$

The tensor multi-rank of $\mathcal{Y} \in \mathbb{R}^{I_1 \times I_2 \times I_3}$ is a vector, denoted as $rank_r(\mathcal{Y}) \in \mathbb{R}^{I_3}$, with the i -th element equals to the rank of i -th frontal slice of \mathcal{Y} .

Definition 10 (Tensor nuclear norm (TNN)): The tensor nuclear norm of a tensor $\mathcal{Y} \in \mathbb{R}^{I_1 \times I_2 \times I_3}$, denoted as $\|\mathcal{Y}\|_{TNN}$, is defined as the sum of the singular values of all the frontal slices of $\tilde{\mathcal{Y}}$, i.e.,

$$\|\mathcal{Y}\|_{TNN} := \sum_{i=1}^{I_3} \|\tilde{\mathcal{Y}}^{(i)}\|_* \quad (5)$$

where $\tilde{\mathcal{Y}}^{(i)}$ is the i -th frontal slice of $\tilde{\mathcal{Y}}$, with $\tilde{\mathcal{Y}} = fft(\mathcal{Y}, [], 3)$.

Definition 11 (N-tubal rank [25]): The N-tubal rank of an Nth-order tensor $\mathcal{Y} \in \mathbb{R}^{I_1 \times I_2 \times \dots \times I_N}$ is defined as a vector, the elements of which contain the tubal rank of all mode- $k_1 k_2$ unfolding tensors, i.e.,

$$N - rank_t(\mathcal{Y}) := (rank_t(\mathcal{Y}_{(12)}), rank_t(\mathcal{Y}_{(13)}), \dots, rank_t(\mathcal{Y}_{(1N)}), rank_t(\mathcal{Y}_{(23)}), \dots, rank_t(\mathcal{Y}_{(2N)}), \dots, rank_t(\mathcal{Y}_{(N-1N)})) \in \mathbb{R}^{N(N-1)/2}. \quad (6)$$

Theorem 2 (Equivalent minimax-concave penalty (EMCP) [33]): Let $\lambda \in \mathbb{R}_{>0}$, $\gamma > 1$ and $y \in \mathbb{R}$. The MCP $h_{\gamma, \lambda} : \mathbb{R} \rightarrow \mathbb{R}_{\geq 0}$ is the solution of the following optimization problem:

$$h_{\gamma, \lambda}(y) = \min_{\omega \in \mathbb{R}_{\geq 0}} \left\{ \omega |y| + \frac{\gamma}{2} (\omega - \lambda)^2 \right\}. \quad (7)$$

III. BIVARIATE EQUIVALENT MINIMAX-CONCAVE PENALTY

In this section, we will construct and obtain the BEMCP theorem, which turns λ and γ into variables at the same time. Then the BEWTGN theorem is applied to tensor singular values to deduce the BEWTGN theorem, and its corresponding properties are analyzed and established.

Theorem 3 (Bivariate Equivalent Minimax-Concave Penalty (BEMCP)): Let $\lambda, v \in \mathbb{R}_{\geq 0}$, $\gamma \in \mathbb{R}_{>1}$ and $y \in \mathbb{R}$. The MCP $h_{\gamma, \lambda} : \mathbb{R} \rightarrow \mathbb{R}_{\geq 0}$ is the solution of the following optimization problem:

$$h_{\gamma, \lambda}(y) = \min_{v \geq 0} \frac{2v|y| + (v - \lambda\gamma)^2}{2\gamma}. \quad (8)$$

Proof: Consider the following function

$$h(y, v) = \frac{2v|y| + (v - \lambda\gamma)^2}{2\gamma}. \quad (9)$$

Let v^* denote the first-order critical point of $h(y, v)$, i.e.,

$$v^* = \arg \min_v h(y, v). \quad (10)$$

Since $h(y, v)$ is differentiable with respect to v , setting

$$\frac{\partial h(y, v)}{\partial v} \Big|_{v=v^*} = 0 \quad (11)$$

gives

$$v^* = \begin{cases} \lambda\gamma - |y|, & |y| \leq \gamma\lambda, \\ 0, & |y| \geq \gamma\lambda. \end{cases} \quad (12)$$

The BEMCP is given by $h_{\gamma, \lambda}(y) = h(y, v^*)$. Substituting for v^* in $h(y, v)$, we get

$$h_{\gamma, \lambda}(y) = \begin{cases} \lambda|y| - \frac{y^2}{2\gamma}, & |y| \leq \gamma\lambda, \\ \frac{\lambda^2}{2\gamma}, & |y| \geq \gamma\lambda. \end{cases} \quad (13)$$

Definition 12 (Weighted Tensor Γ -norm (WTGN)): The tensor Γ -norm of $\mathcal{Y} \in \mathbb{R}^{I_1 \times I_2 \times I_3}$, denoted by $\|\mathcal{Y}\|_{\Gamma, \Lambda}$, is defined as follows:

$$\|\mathcal{Y}\|_{\Gamma, \Lambda} = \sum_{i=1}^{I_3} \sum_{j=1}^R h_{\Gamma(i,j), \Lambda(i,j)} (\sigma_j(\bar{\mathcal{Y}}^{(i)})), \quad (14)$$

where $R = \min(I_1, I_2)$, $\Lambda \in \mathbb{R}_{\geq 0}^{I_3 \times R}$, $\Gamma \in \mathbb{R}_{> 1}^{I_3 \times R}$.

Theorem 4 (Bivariate Equivalent Weighted Tensor Γ -norm (BEWTGN)): For a third-order tensor $\mathcal{Y} \in \mathbb{R}^{I_1 \times I_2 \times I_3}$. Let $\nu, \bar{\Lambda} \in \mathbb{R}_{> 0}^{I_3 \times R}$, $\Gamma \in \mathbb{R}_{> 1}^{I_3 \times R}$, and $R = \min\{I_1, I_2\}$. The weighted tensor Γ -norm is obtained equivalently as

$$\|\mathcal{Y}\|_{\Gamma, \Lambda} = \min_{\nu} \left\{ \|\mathcal{Y}\|_{\frac{\nu}{\Gamma}, *}, * + \frac{1}{2} \left\| \frac{\nu - \Lambda \star \Gamma}{\Gamma \star \Gamma} \right\|_F^2 \right\} \quad (15)$$

where $\|\mathcal{Y}\|_{\frac{\nu}{\Gamma}, *}, * = \sum_{i=1}^{I_3} \sum_{j=1}^R \frac{\nu(i_3, j)}{\Gamma(i_3, j)} \sigma_j(\bar{\mathcal{Y}}^{(i)})$ is the weighted nuclear-norm of i_3 -th slice of $\bar{\mathcal{Y}}$, and $\bar{\mathcal{Y}} = \text{fft}(\mathcal{Y}, [], 3)$.

Proof: The proof is similar to that of Theorem 3, since the objective function in Eq.(15) is non-negative and separable. ■

Remark 1: In particular, when the third dimension I_3 of the third-order tensor \mathcal{Y} is 1, the BEWTGN can degenerate into the form of the bivariate equivalent matrix Γ -norm.

Remark 2: Unlike the nuclear norm penalty, the WTGN(14), and the BEWTGN (15) do not satisfy the triangle inequality. Some important properties of the BEWTGN itself are presented below.

Proposition 1: The BEWTGN defined in (15) satisfies the following properties:

(a) **Non-negativity:** The BEWTGN is non-negative, i.e., $\|\mathcal{Y}\|_{\Gamma, \Lambda} \geq 0$. The equality holds if and only if \mathcal{Y} is the null tensor.

(b) **Concavity:** $\|\mathcal{Y}\|_{\Gamma, \Lambda}$ is concave in the modulus of the singular values of \mathcal{Y} .

(c) **Boundedness:** The BEWTGN is upper-bounded by the weighted nuclear norm, i.e., $\|\mathcal{Y}\|_{\Gamma, \Lambda} \leq \|\mathcal{Y}\|_{\Lambda, *}, *$.

(d) **Asymptotic nuclear norm property:** The BEWTGN approaches the weighted nuclear norm asymptotically, i.e., $\lim_{\Gamma \rightarrow \infty} \|\mathcal{Y}\|_{\Gamma, \Lambda} = \|\mathcal{Y}\|_{\Lambda, *}, *$.

(e) **Unitary invariance:** The BEWTGN is unitary invariant, i.e., $\|\mathcal{U} * \mathcal{Y} * \mathcal{V}\|_{\Gamma, \Lambda} = \|\mathcal{Y}\|_{\Gamma, \Lambda}$, for unitary tensor \mathcal{U} and \mathcal{V} .

Proof: Let

$$p(\mathcal{Y}) = \|\mathcal{Y}\|_{\frac{\nu}{\Gamma}, *}, * + \frac{1}{2} \left\| \frac{\nu - \Lambda \star \Gamma}{\Gamma \star \Gamma} \right\|_F^2.$$

(a) Since $p(\mathcal{Y})$ is the sum of two non-negative functions, $\|\mathcal{Y}\|_{\Gamma, \Lambda} \geq 0$. The equality holds if $\|\mathcal{Y}\|_{\frac{\nu}{\Gamma}, *}, * = 0$, i.e., $\mathcal{Y} = \mathbf{0}$ or $\nu = \mathbf{0}$, the latter being the trivial solution.

(b) The function $p(\mathcal{Y})$ is separable of \mathcal{Y} , i.e.,

$$\begin{aligned} p(\mathcal{Y}) &= \sum_{i_3=1}^{I_3} \sum_{j=1}^R \frac{\nu(i_3, j)}{\Gamma(i_3, j)} \sigma_j(\bar{\mathcal{Y}}^{(i_3)}) + \frac{(\nu(i_3, j) - \Lambda(i_3, j)\Gamma(i_3, j))^2}{2\Gamma(i_3, j)}, \\ &= \sum_{i_3=1}^{I_3} \sum_{j=1}^R p(\sigma_j(\bar{\mathcal{Y}}^{(i_3)})) \end{aligned}$$

Since p is an affine function in $\sigma_j(\bar{\mathcal{Y}}^{(i_3)})$, we can write, for $0 \leq \alpha \leq 1$, that

$$\begin{aligned} &\|(\alpha \mathcal{Y}_1 + (1 - \alpha) \mathcal{Y}_2)_{\Gamma, \Lambda} \\ &= \min_{\nu} p(\alpha \mathcal{Y}_1 + (1 - \alpha) \mathcal{Y}_2) \\ &\geq \min_{\nu} \alpha p(\mathcal{Y}_1) + (1 - \alpha) p(\mathcal{Y}_2) \\ &\geq \min_{\nu} \alpha p(\mathcal{Y}_1) + \min_{\nu} (1 - \alpha) p(\mathcal{Y}_2) \\ &= \alpha \|\mathcal{Y}_1\|_{\Gamma, \Lambda} + (1 - \alpha) \|\mathcal{Y}_2\|_{\Gamma, \Lambda}. \end{aligned}$$

Hence, $\|\mathcal{Y}\|_{\Gamma, \Lambda}$ is concave in the modulus of the singular values of \mathcal{Y} .

(c) For $\gamma > 1$,

$$\|\mathcal{Y}\|_{\Gamma, \Lambda} \leq \|\mathcal{Y}\|_{\frac{\nu}{\Gamma}, *}, * + \frac{1}{2} \left\| \frac{\nu - \Lambda \star \Gamma}{\Gamma \star \Gamma} \right\|_F^2, \quad \forall \nu \in \mathbb{R}_{\geq 0}^{I_3 \times R}.$$

Therefore, the above inequality holds true even for $\nu = \Lambda \star \Gamma$, which leads to $\|\mathcal{Y}\|_{\Gamma, \Lambda} \leq \|\mathcal{Y}\|_{\frac{\nu}{\Gamma}, *}, *$.

(d) As $\Gamma \rightarrow \infty$, the optimal ν in (15) is $\Lambda \star \Gamma$. Therefore,

$$\lim_{\Gamma \rightarrow \infty} \|\mathcal{Y}\|_{\Gamma, \Lambda} = \|\mathcal{Y}\|_{\frac{\nu}{\Gamma}, *}, *$$

(e) Consider the definition of the tensor weighted nuclear norm

$$\|\mathcal{Y}\|_{\frac{\nu}{\Gamma}, *}, * := \sum_{i=1}^{I_3} \sum_{j=1}^R \frac{\nu(i, j)}{\Gamma(i, j)} \sigma_j(\bar{\mathcal{Y}}^{(i)}), \quad (16)$$

where $\sigma(\bar{\mathcal{Y}}^{(i)})$ denote the singular values of i th slice of $\bar{\mathcal{Y}}$. Let $w = \frac{\nu}{\Gamma}$, we can express

$$\|\mathcal{Y}\|_{w, *}, * = \sum_{i=1}^{I_3} \text{Tr}(\text{diag}(w(i, :)) \sqrt{\bar{\mathcal{Y}}^{(i)T} \bar{\mathcal{Y}}^{(i)}}), \quad (17)$$

where $\text{diag}(w(i, :))$ denotes a diagonal matrix with diagonal entries coming from the elements of i th column vector of w , and $\text{Tr}(\cdot)$ denotes the Trace operator.

Next, consider $\|\mathcal{U} * \mathcal{Y} * \mathcal{V}\|_{w, *}, *$, where \mathcal{U} and \mathcal{V} are unitary tensors:

$$\begin{aligned} \|\mathcal{U} * \mathcal{Y} * \mathcal{V}\|_{w, *}, * &:= \sum_{i=1}^{I_3} \|\bar{\mathcal{U}}^{(i)} \bar{\mathcal{Y}}^{(i)} \bar{\mathcal{V}}^{(i)}\|_{w(i, :), *}, * \\ &= \sum_{i=1}^{I_3} \text{Tr}(\text{diag}(w(i, :)) \sqrt{(\bar{\mathcal{U}}^{(i)} \bar{\mathcal{Y}}^{(i)} \bar{\mathcal{V}}^{(i)})^T (\bar{\mathcal{U}}^{(i)} \bar{\mathcal{Y}}^{(i)} \bar{\mathcal{V}}^{(i)})}). \end{aligned} \quad (18)$$

Properties of the tensor generated by performing discrete Fourier transformation (DFT) show that $\bar{\mathcal{U}}^{(i)}$ and $\bar{\mathcal{V}}^{(i)}$ are unitary matrices. Then, we get the following formula:

$$\|\mathcal{U} * \mathcal{Y} * \mathcal{V}\|_{w, *}, * = \|\mathcal{Y}\|_{w, *}, *. \quad (19)$$

Based on (19), we can express

$$\begin{aligned} &\|\mathcal{U} * \mathcal{Y} * \mathcal{V}\|_{\Gamma, \Lambda} \\ &= \min_{\nu} \left\{ \|\mathcal{U} * \mathcal{Y} * \mathcal{V}\|_{\frac{\nu}{\Gamma}, *}, * + \frac{1}{2} \left\| \frac{\nu - \Lambda \star \Gamma}{\Gamma \star \Gamma} \right\|_F^2 \right\} \\ &= \min_{\nu} \left\{ \|\mathcal{Y}\|_{\frac{\nu}{\Gamma}, *}, * + \frac{1}{2} \left\| \frac{\nu - \Lambda \star \Gamma}{\Gamma \star \Gamma} \right\|_F^2 \right\} \\ &= \|\mathcal{Y}\|_{\Gamma, \Lambda}, \end{aligned}$$

which is the BEWTGN. This establishes the unitary invariance of the BEWTGN. ■

IV. PROXIMAL OPERATORS FOR THE BEMCP THEOREM AND BEWTGN

In this section, to solve the model established based on the BEMCP theorem, we present the proximal operators for the BEMCP theorem and BEWTGN.

Theorem 5 (Proximal operator for the BEMCP): Consider the BEMCP given in (8). Its proximal operator denoted by $P_{\gamma,\lambda} : \mathbb{R} \rightarrow \mathbb{R}$, $\gamma \in \mathbb{R}_{>1}$, $\lambda \in \mathbb{R}_{\geq 0}$ and defined as follows:

$$P_{\gamma,\lambda}(y) = \arg \min_g \left\{ \frac{1}{2}(g-y)^2 + h_{\gamma,\lambda}(g) \right\}, \quad (20)$$

is given by

$$P_{\gamma,\lambda}(y) = \min \left(|y|, \max \left(\frac{\gamma(|y| - \lambda)}{\gamma - 1}, 0 \right) \right) \text{sign}(y). \quad (21)$$

Proof: Let

$$\begin{aligned} P_{\gamma,\lambda}(y) &= \arg \min_g \left\{ \frac{1}{2}(g-y)^2 + \min_{v \geq 0} \left\{ \frac{2v|g| + (v - \lambda\gamma)^2}{2\gamma} \right\} \right\}, \\ &= \arg \min_g \left\{ \frac{1}{2}(g-y)^2 + h(g, v^*) \right\}, \end{aligned}$$

where

$$v^* = \arg \min_{v \geq 0} h(g, v) = \max(\lambda\gamma - |g|, 0).$$

We must now determine $P_{\gamma,\lambda}(y)$ for a given v^* . This is derived considering various values that v^* can take:

(1) Case1: $v^* = 0$. Correspondingly, $h(g, v^*) = \frac{\lambda^2\gamma}{2}$, and then

$$P_{\gamma,\lambda}(y) = \arg \min_g \left\{ \frac{1}{2}(g-y)^2 + \frac{\lambda^2\gamma}{2} \right\} = y.$$

The condition $v^* = 0$ translates to $|g| \geq \lambda\gamma$, therefore,

$$P_{\gamma,\lambda}(y) = y, \quad \text{for } |g| \geq \lambda\gamma. \quad (22)$$

(2) Case2: $0 < v^* < \lambda\gamma$. By definition of v^* , we have that

$$v^* = \lambda\gamma - |g|, \quad |g| \leq \lambda\gamma. \quad (23)$$

Further, considering $0 < g \leq \lambda\gamma$ gives $v^* = \lambda\gamma - g$, which result in

$$\begin{aligned} P_{\gamma,\lambda}(y) &= \arg \min_g \left\{ \frac{1}{2}(g-y)^2 + \frac{2v^*g + (v^* - \lambda\gamma)^2}{2\gamma} \right\}, \\ &= \frac{\gamma}{\gamma-1}(y-\lambda) \quad \text{for } \lambda < y < \lambda\gamma. \end{aligned}$$

Similarly, considering $-\lambda\gamma \leq g < 0$ gives $v^* = \lambda\gamma + g$, which result in

$$\begin{aligned} P_{\gamma,\lambda}(y) &= \arg \min_g \left\{ \frac{1}{2}(g-y)^2 + \frac{2v^*(-g) + (v^* - \lambda\gamma)^2}{2\gamma} \right\}, \\ &= \frac{\gamma}{\gamma-1}(-y-\lambda) \quad \text{for } -\lambda\gamma < y < -\lambda. \end{aligned}$$

Combining the two expressions brings

$$P_{\gamma,\lambda}(y) = \frac{\gamma}{\gamma-1}(|y| - \lambda)\text{sign}(y), \quad \text{for } \lambda < |y| < \lambda\gamma. \quad (24)$$

(3) Case3: $v^* = \lambda\gamma$. This induces $g = 0$, which implies

$P_{\gamma,\lambda}(y) = 0$. Substituting $v^* = \lambda\gamma$ in the definition of $P_{\gamma,\lambda}(y)$ gives

$$0 = \arg \min_g \left\{ \frac{1}{2}(g-y)^2 + \lambda|g| \right\}.$$

Considering the subdifferential, we get $0 \in -y + \lambda\partial|g|$, or equivalently, $|y| \leq \lambda$. Therefore,

$$P_{\gamma,\lambda}(y) = 0, \quad \text{for } |y| \leq \lambda. \quad (25)$$

Combining equations (22), (24), and (25) yields

$$P_{\gamma,\lambda}(y) = \min \left(|y|, \max \left(\frac{\gamma(|y| - \lambda)}{\gamma - 1}, 0 \right) \right) \text{sign}(y). \quad (26)$$

Theorem 6 (Proximal operator for the BEWTGN): Consider the BEWTGN given in (15). Its proximal operator denoted by $S_{\Gamma,\Lambda} : \mathbb{R}^{I_1 \times I_2 \times I_3} \rightarrow \mathbb{R}^{I_1 \times I_2 \times I_3}$, $\Gamma \in \mathbb{R}_{>1}^{R \times I_3}$, $\bar{\Lambda} \in \mathbb{R}_{\geq 0}^{R \times I_3}$, $R = \min\{I_1, I_2\}$ and defined as follows:

$$S_{\Gamma,\Lambda}(\mathcal{Y}) = \arg \min_{\mathcal{L}} \left\{ \frac{1}{2} \|\mathcal{L} - \mathcal{Y}\|_F^2 + \|\mathcal{L}\|_{\Gamma,\Lambda} \right\}, \quad (27)$$

is given by

$$S_{\Gamma,\Lambda}(\mathcal{Y}) = \mathcal{U} * \mathcal{S}_1 * \mathcal{V}^H. \quad (28)$$

where \mathcal{U} and \mathcal{V} are derived from the t-SVD of $\mathcal{Y} = \mathcal{U} * \mathcal{S}_2 * \mathcal{V}^H$. More importantly, the i th front slice of DFT of \mathcal{S}_1 and \mathcal{S}_2 , i.e., $\bar{\mathcal{S}}_1^{(i)} = \sigma(\bar{\mathcal{L}}^{(i)})$ and $\bar{\mathcal{S}}_2^{(i)} = \sigma(\bar{\mathcal{Y}}^{(i)})$, has the following relationship:

$$\sigma(\bar{\mathcal{L}}^{(i)}) = \min \left\{ \sigma(\bar{\mathcal{Y}}^{(i)}), \max \left\{ \frac{\Gamma_{(i,:)}(\sigma(\bar{\mathcal{Y}}^{(i)}) - \Lambda_{(i,:)})}{\Gamma_{(i,:)} - 1}, 0 \right\} \right\}.$$

Proof: Let $\mathcal{Y} = \mathcal{U} * \mathcal{S}_2 * \mathcal{V}^H$ and $\mathcal{L} = \mathcal{W} * \mathcal{S}_1 * \mathcal{R}^H$ be the t-SVD of \mathcal{Y} and \mathcal{L} , respectively. Consider

$$\begin{aligned} S_{\Gamma,\Lambda}(\mathcal{Y}) &= \arg \min_{\mathcal{L}} \frac{1}{2} \|\mathcal{L} - \mathcal{Y}\|_F^2 + \|\mathcal{L}\|_{\Gamma,\Lambda} \\ &= \arg \min_{\mathcal{L}} \frac{1}{2} \|\mathcal{W} * \mathcal{S}_1 * \mathcal{R}^H - \mathcal{U} * \mathcal{S}_2 * \mathcal{V}^H\|_F^2 \\ &\quad + \|\mathcal{L}\|_{\Gamma,\Lambda} \\ &= \arg \min_{\bar{\mathcal{L}}} \sum_{i=1}^{I_3} \frac{1}{2} \|\bar{\mathcal{W}}^{(i)} * \bar{\mathcal{S}}_1^{(i)} * \bar{\mathcal{R}}^{(i)H} - \bar{\mathcal{U}}^{(i)} \\ &\quad * \bar{\mathcal{S}}_2^{(i)} * \bar{\mathcal{V}}^{(i)H}\|_F^2 + \|\bar{\mathcal{L}}^{(i)}\|_{\Gamma_{(i,:)}, \Lambda_{(i,:)}}. \end{aligned} \quad (29)$$

It can be found that (29) is separable and can be divided into I_3 sub-problems. For the i th sub-problem:

$$\begin{aligned} &\arg \min_{\bar{\mathcal{L}}^{(i)}} \frac{1}{2} \|\bar{\mathcal{W}}^{(i)} * \bar{\mathcal{S}}_1^{(i)} * \bar{\mathcal{R}}^{(i)H} - \bar{\mathcal{U}}^{(i)} * \bar{\mathcal{S}}_2^{(i)} * \bar{\mathcal{V}}^{(i)H}\|_F^2 \\ &\quad + \|\bar{\mathcal{L}}^{(i)}\|_{\Gamma_{(i,:)}, \Lambda_{(i,:)}} \\ &= \arg \min_{\bar{\mathcal{L}}^{(i)}} \frac{1}{2} \text{Tr}(\bar{\mathcal{S}}_1^{(i)} \bar{\mathcal{S}}_1^{(i)H}) + \frac{1}{2} \text{Tr}(\bar{\mathcal{S}}_2^{(i)} \bar{\mathcal{S}}_2^{(i)H}) \\ &\quad + \text{Tr}(\bar{\mathcal{L}}^{(i)H} \bar{\mathcal{Y}}^{(i)}) + \|\bar{\mathcal{L}}^{(i)}\|_{\Gamma_{(i,:)}, \Lambda_{(i,:)}}. \end{aligned} \quad (30)$$

Invoking von Neumann's trace inequality [38], we can write

$$\begin{aligned}
& \arg \min_{\bar{\mathcal{L}}^{(i)}} \frac{1}{2} \|\bar{\mathcal{W}}^{(i)} * \bar{\mathcal{S}}_1^{(i)} * \bar{\mathcal{R}}^{(i)H} - \bar{\mathcal{U}}^{(i)} * \bar{\mathcal{S}}_2^{(i)} * \bar{\mathcal{V}}^{(i)H}\|_F^2 \\
& + \|\bar{\mathcal{L}}^{(i)}\|_{\Gamma_{(i,:), \Lambda_{(i,:)}}} \\
& \geq \arg \min_{\bar{\mathcal{S}}_1^{(i)}} \frac{1}{2} \text{Tr}(\bar{\mathcal{S}}_1^{(i)} \bar{\mathcal{S}}_1^{(i)H}) + \frac{1}{2} \text{Tr}(\bar{\mathcal{S}}_2^{(i)} \bar{\mathcal{S}}_2^{(i)H}) \\
& + \text{Tr}(\bar{\mathcal{S}}_2^{(i)} \bar{\mathcal{S}}_1^{(i)H}) + \|\bar{\mathcal{L}}^{(i)}\|_{\Gamma_{(i,:), \Lambda_{(i,:)}}} \\
& = \arg \min_{\sigma(\bar{\mathcal{L}}^{(i)})} \frac{1}{2} \|\sigma(\bar{\mathcal{L}}^{(i)}) - \sigma(\bar{\mathcal{Y}}^{(i)})\|_F^2 + \|\bar{\mathcal{L}}^{(i)}\|_{\Gamma_{(i,:), \Lambda_{(i,:)}}}.
\end{aligned}$$

The equality holds when $\bar{\mathcal{W}}^{(i)} = \bar{\mathcal{U}}^{(i)}$ and $\bar{\mathcal{R}}^{(i)} = \bar{\mathcal{V}}^{(i)}$. Therefore, the optimal solution to (29) is obtained by solving the problem given below:

$$\sigma(\bar{\mathcal{L}}^{(i)}) = \min \left\{ \sigma(\bar{\mathcal{Y}}^{(i)}), \max \left\{ \frac{\Gamma_{(i,:)}(\sigma(\bar{\mathcal{Y}}^{(i)}) - \Lambda_{(i,:)})}{\Gamma_{(i,:)} - 1}, 0 \right\} \right\}.$$

V. THE BEMCP MODELS AND SOLVING ALGORITHMS

In this section, in order to better verify the superiority of our BEMCP theorem, before giving the BEMCP model based on the N-tubal rank, we first review the models of traditional MCP and EMCP based on the N-tubal rank. And the traditional MCP model based on N-tubal rank is called the NCMP model.

$$\min_{\mathcal{X}} \sum_{1 \leq l_1 < l_2 \leq N} \alpha_{l_1 l_2} \|\mathcal{X}_{(l_1 l_2)}\|_* \quad \text{s.t.} \quad \mathcal{P}_{\Omega}(\mathcal{X} - \mathcal{Z}) = \mathbf{0}, \quad (31)$$

Applying different MCP non-convex functions to singular values of problem (31) leads to the following model.

A. The NMCP model

Using the MCP function, we get the following optimization model:

$$\min_{\mathcal{X}} \sum_{1 \leq l_1 < l_2 \leq N} \alpha_{l_1 l_2} \|\mathcal{X}_{(l_1 l_2)}\|_{\gamma, \lambda} \quad \text{s.t.} \quad \mathcal{P}_{\Omega}(\mathcal{X} - \mathcal{Z}) = \mathbf{0}. \quad (32)$$

Under the framework of alternation direction method of multipliers (ADMM) [34], [35], [39], the easy-to-implement optimization strategy could be provided to solve (32). We introduce a set of tensors $\{\mathcal{Y}_{l_1 l_2} = \mathcal{X}\}_{1 \leq l_1 < l_2 \leq N}^N$ and transfer optimization problem (32), in its augmented Lagrangian form, as follows:

$$\begin{aligned}
& J(\mathcal{X}, \mathcal{Y}, \mathcal{Q}) \\
& = \sum_{1 \leq l_1 < l_2 \leq N} \alpha_{l_1 l_2} \|\mathcal{Y}_{l_1 l_2(l_1 l_2)}\|_{\gamma, \lambda} + \frac{\rho_{l_1 l_2}}{2} \|\mathcal{X} - \mathcal{Y}_{l_1 l_2} + \frac{\mathcal{Q}_{l_1 l_2}}{\rho_{l_1 l_2}}\|_F^2 \\
& \quad \text{s.t.} \quad \mathcal{P}_{\Omega}(\mathcal{X} - \mathcal{Z}) = \mathbf{0}, \quad (33)
\end{aligned}$$

where $\{\mathcal{Q}_{l_1 l_2}\}_{1 \leq l_1 < l_2 \leq N}^N$ are tensor Lagrangian multiplier sets; $\{\rho_{l_1 l_2}\}_{1 \leq l_1 < l_2 \leq N}^N > 0$ are the augmented Lagrangian parameters; $\alpha_{l_1 l_2} \geq 0$ are N-tubal rank weights and $\sum_{1 \leq l_1 < l_2 \leq N}^N \alpha_{l_1 l_2} = 1$. Besides, variables \mathcal{X} , \mathcal{Y} , \mathcal{Q} are updated alternately in the order of $\mathcal{Y} \rightarrow \mathcal{X} \rightarrow \mathcal{Q}$. For convenience, we mark the updated

variable as $(\cdot)^+$. The update equations are acquired in the following.

Update \mathcal{Y} : Fix other variables, and the corresponding optimization is as follows:

$$\mathcal{Y}_{l_1 l_2}^+ = \arg \min_{\mathcal{Y}_{l_1 l_2}} \alpha_{l_1 l_2} \|\mathcal{Y}_{l_1 l_2(l_1 l_2)}\|_{\gamma, \lambda} + \frac{\rho_{l_1 l_2}}{2} \|\mathcal{X} - \mathcal{Y}_{l_1 l_2} + \frac{\mathcal{Q}_{l_1 l_2}}{\rho_{l_1 l_2}}\|_F^2.$$

Calling Theorem 6, the solution to the above optimization is given by:

$$\mathcal{Y}_{l_1 l_2}^+ = S_{\frac{\gamma \rho_{l_1 l_2}}{\alpha_{l_1 l_2}}, \frac{\lambda \rho_{l_1 l_2}}{\alpha_{l_1 l_2}}} \left(\mathcal{X} + \frac{\mathcal{Q}_{l_1 l_2}}{\rho_{l_1 l_2}} \right), \quad (34)$$

where S denotes the proximal operator defined in (28).

Update \mathcal{X} : The closed form of \mathcal{X} can be acquired by setting the derivative of (33) to zero. We can now update \mathcal{X} by the following equation:

$$\mathcal{X}^+ = \mathcal{P}_{\Omega^c} \left(\frac{\sum_{1 \leq l_1 < l_2 \leq N} \rho_{l_1 l_2} (\mathcal{Y}_{l_1 l_2} - \frac{\mathcal{Q}_{l_1 l_2}}{\rho_{l_1 l_2}})}{\sum_{1 \leq l_1 < l_2 \leq N} \rho_{l_1 l_2}} \right) + \mathcal{P}_{\Omega}(\mathcal{Z}). \quad (35)$$

Update \mathcal{Q} : Finally, multipliers $\mathcal{Q}_{l_1 l_2}$ are updated as follows:

$$\mathcal{Q}_{l_1 l_2}^+ = \mathcal{Q}_{l_1 l_2} + \rho_{l_1 l_2} (\mathcal{X} - \mathcal{Y}_{l_1 l_2}). \quad (36)$$

The optimization steps of the NMCP formulation are listed in Algorithm 1.

Algorithm 1 NMCP

Input: An incomplete tensor \mathcal{Z} , the index set of the known elements Ω , convergence criteria ϵ , maximum iteration number K .

Initialization: $\mathcal{X}^0 = \mathcal{Z}_{\Omega}$, $\mathcal{Y}_{l_1 l_2}^0 = \mathcal{X}^0$, $\rho_{l_1 l_2}^0 > 0$, $\mu > 1$.

while not converged and $k < K$ **do**

 Updating $\mathcal{Y}_{l_1 l_2}^k$ via (34);

 Updating \mathcal{X}^k via (35);

 Updating the multipliers $\mathcal{Q}_{l_1 l_2}^k$ via (36);

$\rho_{l_1 l_2}^k = \mu \rho_{l_1 l_2}^{k-1}$, $k = k + 1$;

 Check the convergence conditions $\|\mathcal{X}^{k+1} - \mathcal{X}^k\|_{\infty} \leq \epsilon$.

end while

return \mathcal{X}^{k+1} .

Output: Completed tensor $\mathcal{X} = \mathcal{X}^{k+1}$.

B. The EMCP model

Similarly, using the EMCP Theorem, we get the following optimization model:

$$\min_{\mathcal{X}} \sum_{1 \leq l_1 < l_2 \leq N} \alpha_{l_1 l_2} \|\mathcal{X}_{(l_1 l_2)}\|_{\gamma, \bar{\Lambda}_{(l_1 l_2)}} \quad \text{s.t.} \quad \mathcal{P}_{\Omega}(\mathcal{X} - \mathcal{Z}) = \mathbf{0}. \quad (37)$$

Under the framework of the alternation direction method of multipliers (ADMM), the easy-to-implement optimization strategy could be provided to solve (37). We introduce a set of tensors $\{\mathcal{Y}_{l_1 l_2} = \mathcal{X}\}_{1 \leq l_1 < l_2 \leq N}^N$ and transfer optimization problem (37), in its augmented Lagrangian form, as follows:

$$\begin{aligned}
& J(\mathcal{X}, \mathcal{Y}, \bar{\Lambda}, W, \mathcal{Q}) \\
& = \sum_{1 \leq l_1 < l_2 \leq N} \alpha_{l_1 l_2} \|\mathcal{Y}_{l_1 l_2(l_1 l_2)}\|_{\gamma, \bar{\Lambda}_{(l_1 l_2)}} \\
& + \frac{\rho_{l_1 l_2}}{2} \|\mathcal{X} - \mathcal{Y}_{l_1 l_2} + \frac{\mathcal{Q}_{l_1 l_2}}{\rho_{l_1 l_2}}\|_F^2 \quad \text{s.t.} \quad \mathcal{P}_{\Omega}(\mathcal{X} - \mathcal{Z}) = \mathbf{0}
\end{aligned} \quad (38)$$

where \mathcal{Y} and \mathcal{Q} are tensor sets; $\bar{\Lambda}$ and W are matrix sets; $\{\mathcal{Y}_{l_1 l_2} = \mathcal{X}\}_{1 \leq l_1 < l_2 \leq N}$; $\{\mathcal{Q}_{l_1 l_2}\}_{1 \leq l_1 < l_2 \leq N}$ are Lagrangian multipliers; $\{\bar{\Lambda}, W\}_{1 \leq l_1 < l_2 \leq N} \in \mathbb{R}^{I_3 \times R}$ are MCP variable and weight sets, respectively; $\{\rho_{l_1 l_2}\}_{1 \leq l_1 < l_2 \leq N} > 0$ are the augmented Lagrangian parameters; $\alpha_{l_1 l_2} \geq 0$ are weights and $\sum_{1 \leq l_1 < l_2 \leq N} \alpha_{l_1 l_2} = 1$.

Besides, variables \mathcal{X} , \mathcal{Y} , $\bar{\Lambda}$, W , \mathcal{Q} are updated alternately in the order of $\mathcal{Y} \rightarrow W \rightarrow \bar{\Lambda} \rightarrow \mathcal{X} \rightarrow \mathcal{Q}$. The update equations are acquired in the following.

Update \mathcal{Y} : Fix other variables, and the corresponding optimization is as follows:

$$\begin{aligned} \mathcal{Y}_{l_1 l_2}^+ &= \arg \min_{\mathcal{Y}_{l_1 l_2}} \alpha_{l_1 l_2} \|\mathcal{Y}_{l_1 l_2}(l_1 l_2)\|_{\gamma, \bar{\Lambda}_{l_1 l_2}} \\ &\quad + \frac{\rho_{l_1 l_2}}{2} \|\mathcal{X} - \mathcal{Y}_{l_1 l_2} + \frac{\mathcal{Q}_{l_1 l_2}}{\rho_{l_1 l_2}}\|_F^2. \end{aligned}$$

Invoking Theorem 6, the solution to the above optimization is given by:

$$\mathcal{Y}_{l_1 l_2}^+ = S_{\frac{\gamma \rho_{l_1 l_2}}{\alpha_{l_1 l_2}}, \frac{\bar{\Lambda}_{l_1 l_2} \rho_{l_1 l_2}}{\alpha_{l_1 l_2}}} \left(\mathcal{X} + \frac{\mathcal{Q}_{l_1 l_2}}{\rho_{l_1 l_2}} \right), \quad (39)$$

where S denotes the proximal operator defined in (28).

Update W : Retaining only those components in $\mathcal{Y}_{l_1 l_2}$ in (38) that depend on $W_{l_1 l_2}$, we write

$$W_{l_1 l_2}^+ = \arg \min_{W_{l_1 l_2}} \sum_{i_3=1}^{I_3} \|\bar{\mathcal{Y}}_{l_1 l_2}^{(i_3)}\|_{W_{l_1 l_2}(i_3, \cdot)} + \frac{\gamma}{2} \|W_{l_1 l_2} - \bar{\Lambda}_{l_1 l_2}\|_F^2,$$

which has the following closed-form solution:

$$W_{l_1 l_2}^+(i_3, \cdot) = \max(\bar{\Lambda}_{l_1 l_2}(i_3, \cdot) - \frac{\sigma(\mathcal{Y}_{l_1 l_2}^{+(i_3)})}{\gamma}, 0). \quad (40)$$

Update $\bar{\Lambda}$: The update for $\bar{\Lambda}_{l_1 l_2}$ has the following closed-form solution:

$$\bar{\Lambda}_{l_1 l_2}^+ = \arg \min_{\bar{\Lambda}_{l_1 l_2}} \|W_{l_1 l_2} - \bar{\Lambda}_{l_1 l_2}\|_F^2 = W_{l_1 l_2}^+. \quad (41)$$

Update \mathcal{X} : The closed form of \mathcal{X} can be acquired by setting the derivative of (38) to zero. We can now update \mathcal{X} by the following equation:

$$\mathcal{X}^+ = \mathcal{P}_{\Omega^c} \left(\frac{\sum_{1 \leq l_1 < l_2 \leq N} \rho_{l_1 l_2} (\mathcal{Y}_{l_1 l_2} - \frac{\mathcal{Q}_{l_1 l_2}}{\rho_{l_1 l_2}})}{\sum_{1 \leq l_1 < l_2 \leq N} \rho_{l_1 l_2}} \right) + \mathcal{P}_{\Omega}(\mathcal{Z}). \quad (42)$$

Update \mathcal{Q} : Finally, multipliers $\mathcal{Q}_{l_1 l_2}$ are updated as follows:

$$\mathcal{Q}_{l_1 l_2}^+ = \mathcal{Q}_{l_1 l_2} + \rho_{l_1 l_2} (\mathcal{X} - \mathcal{Y}_{l_1 l_2}). \quad (43)$$

The optimization steps of the EMCP formulation are listed in Algorithm 2.

C. The BEMCP model

Using the BEMCP Theorem, we get the following optimization model:

$$\min_{\mathcal{X}} \sum_{1 \leq l_1 < l_2 \leq N} \alpha_{l_1 l_2} \|\mathcal{X}(l_1 l_2)\|_{\Gamma_{l_1 l_2}, \Lambda_{l_1 l_2}} \text{ s.t. } \mathcal{P}_{\Omega}(\mathcal{X} - \mathcal{Z}) = \mathbf{0}. \quad (44)$$

Under the framework of the ADMM, the easy-to-implement optimization strategy could be provided to solve (44). We

Algorithm 2 EMCP

Input: An incomplete tensor \mathcal{Z} , the index set of the known elements Ω , convergence criteria ϵ , maximum iteration number K .

Initialization: $\mathcal{X}^0 = \mathcal{Z}_{\Omega}$, $\mathcal{Y}_{l_1 l_2}^0 = \mathcal{X}^0$, $\rho_{l_1 l_2}^0 > 0$, $\mu > 1$.

while not converged and $k < K$ **do**

 Updating $\mathcal{Y}_{l_1 l_2}^k$ via (39);

 Updating $W_{l_1 l_2}^k$ via (40);

 Updating $\bar{\Lambda}_{l_1 l_2}^k$ via (41);

 Updating \mathcal{X}^k via (42);

 Updating the multipliers $\mathcal{Q}_{l_1 l_2}^k$ via (43);

$\rho_{l_1 l_2}^k = \mu \rho_{l_1 l_2}^{k-1}$, $k = k + 1$;

 Check the convergence conditions $\|\mathcal{X}^{k+1} - \mathcal{X}^k\|_{\infty} \leq \epsilon$.

end while

return \mathcal{X}^{k+1} .

Output: Completed tensor $\mathcal{X} = \mathcal{X}^{k+1}$.

introduce a set of tensors $\{\mathcal{Y}_{l_1 l_2} = \mathcal{X}\}_{1 \leq l_1 < l_2 \leq N}$ and transform optimization problem (44), in its augmented Lagrangian form, as follows:

$$\begin{aligned} J(\mathcal{X}, \mathcal{Y}, \Lambda, \Gamma, \nu, \mathcal{Q}) &= \sum_{1 \leq l_1 < l_2 \leq N} \alpha_{l_1 l_2} \|\mathcal{Y}_{l_1 l_2}(l_1 l_2)\|_{\Gamma_{l_1 l_2}, \Lambda_{l_1 l_2}} \\ &\quad + \frac{\rho_{l_1 l_2}}{2} \|\mathcal{X} - \mathcal{Y}_{l_1 l_2} + \frac{\mathcal{Q}_{l_1 l_2}}{\rho_{l_1 l_2}}\|_F^2 \quad \text{s.t.} \quad \mathcal{P}_{\Omega}(\mathcal{X} - \mathcal{Z}) = \mathbf{0}, \end{aligned} \quad (45)$$

where \mathcal{Y} and \mathcal{Q} are tensor sets; Λ, Γ, ν are matrix sets; $\{\mathcal{Y}_{l_1 l_2} = \mathcal{X}\}_{1 \leq l_1 < l_2 \leq N}$; $\{\mathcal{Q}_{l_1 l_2}\}_{1 \leq l_1 < l_2 \leq N}$ are Lagrangian multipliers; $\{\Lambda, \Gamma, \nu\}_{1 \leq l_1 < l_2 \leq N} \in \mathbb{R}^{I_3 \times R}$ are MCP variable sets; $\{\rho_{l_1 l_2}\}_{1 \leq l_1 < l_2 \leq N} > 0$ are the augmented Lagrangian parameters; $\alpha_{l_1 l_2} \geq 0$ are weights and $\sum_{1 \leq l_1 < l_2 \leq N} \alpha_{l_1 l_2} = 1$.

Besides, variables $\mathcal{X}, \mathcal{Y}, \Lambda, \Gamma, \nu, \mathcal{Q}$ are updated alternately in the order of $\mathcal{Y} \rightarrow \nu \rightarrow \Lambda \rightarrow \Gamma \rightarrow \mathcal{X} \rightarrow \mathcal{Q}$. The update equations are derived in the following.

Update \mathcal{Y} : Fix other variables, and the corresponding optimization are as follows:

$$\begin{aligned} \mathcal{Y}_{l_1 l_2}^+ &= \arg \min_{\mathcal{Y}_{l_1 l_2}} \alpha_{l_1 l_2} \|\mathcal{Y}_{l_1 l_2}(l_1 l_2)\|_{\Gamma_{l_1 l_2}, \Lambda_{l_1 l_2}} \\ &\quad + \frac{\rho_{l_1 l_2}}{2} \|\mathcal{X} - \mathcal{Y}_{l_1 l_2} + \frac{\mathcal{Q}_{l_1 l_2}}{\rho_{l_1 l_2}}\|_F^2. \end{aligned}$$

Calling Theorem 6, the solution to the above optimization is given by:

$$\mathcal{Y}_{l_1 l_2}^+ = S_{\frac{\Gamma_{l_1 l_2} \rho_{l_1 l_2}}{\alpha_{l_1 l_2}}, \frac{\Lambda_{l_1 l_2} \rho_{l_1 l_2}}{\alpha_{l_1 l_2}}} \left(\mathcal{X} + \frac{\mathcal{Q}_{l_1 l_2}}{\rho_{l_1 l_2}} \right), \quad (46)$$

where S denotes the proximal operator defined in (28).

Update ν : Retaining only those components in $\mathcal{Y}_{l_1 l_2}$ in (45) that depend on $\nu_{l_1 l_2}$, we write

$$\nu_{l_1 l_2}^+ = \arg \min_{\nu_{l_1 l_2}} \|\mathcal{Y}_{l_1 l_2}(l_1 l_2)\|_{\frac{\nu_{l_1 l_2}}{\Gamma_{l_1 l_2}}, \star} + \frac{1}{2} \left\| \frac{\nu_{l_1 l_2} - \Lambda_{l_1 l_2} \star \Gamma_{l_1 l_2}}{\Gamma_{l_1 l_2} \star \Gamma_{l_1 l_2}} \right\|_F^2,$$

which has the following closed-form solution:

$$\nu_{l_1 l_2}^+(i_3, \cdot) = \max(\Lambda_{l_1 l_2}(i_3, \cdot) \Gamma_{l_1 l_2}(i_3, \cdot) - \sigma(\mathcal{Y}_{l_1 l_2}^{+(i_3)}), \bar{\epsilon}), \quad (47)$$

where the element values of vector $\bar{\epsilon}$ are all small values close to 0, which will avoid the situation where Λ becomes 0 and Γ cannot be solved.

Update Λ : The update for $\Lambda_{l_1 l_2}$ has the following closed-form solution:

$$\Lambda_{l_1 l_2}^+ = \arg \min_{\Lambda_{l_1 l_2}} \left\| \frac{v_{l_1 l_2} - \Lambda_{l_1 l_2} \star \Gamma_{l_1 l_2}}{\Gamma_{l_1 l_2} \star \Gamma_{l_1 l_2}} \right\|_F^2 = \frac{v_{l_1 l_2}^+}{\Gamma_{l_1 l_2}}. \quad (48)$$

Update Γ : The update for $\Gamma_{l_1 l_2}$ has the following closed-form solution:

$$\Gamma_{l_1 l_2}^+ = \arg \min_{\Gamma_{l_1 l_2}} \left\| \mathcal{Y}_{l_1 l_2}^+ \right\|_{\frac{v_{l_1 l_2}^+}{\Gamma_{l_1 l_2}^+}} + \frac{1}{2} \left\| \frac{v_{l_1 l_2}^+ - \Lambda_{l_1 l_2}^+ \star \Gamma_{l_1 l_2}}{\Gamma_{l_1 l_2} \star \Gamma_{l_1 l_2}} \right\|_F^2. \quad (49)$$

Problem (49) is element-wise separable, and by proposition 1 we have the following results:

$$\begin{aligned} & \|\mathcal{Y}\|_{\Gamma_{l_1 l_2}, \Lambda_{l_1 l_2}} \\ &= \sum_{i=1}^{I_3} \sum_{j=1}^R \frac{2v_{(i,j)} \sigma_j(\bar{\mathcal{Y}}^{(i)}) + (v_{(i,j)} - \Lambda_{(i,j)} \Gamma_{(i,j)})^2}{2\Gamma_{(i,j)}}. \end{aligned}$$

Then, we consider the case of one of the elements individually:

$$\frac{2v_{(i,j)} \sigma_j(\bar{\mathcal{Y}}^{(i)}) + (v_{(i,j)} - \Lambda_{(i,j)} \Gamma_{(i,j)})^2}{2\Gamma_{(i,j)}}. \quad (50)$$

The closed form of $\Gamma_{(i,j)}$ can be derived by setting the derivative of (50) to zero:

$$\frac{(\Lambda_{(i,j)} \Gamma_{(i,j)})^2 - 2v_{(i,j)} \sigma_j(\bar{\mathcal{Y}}^{(i)}) - v_{(i,j)}^2}{2\Gamma_{(i,j)}^2} = 0.$$

So, $\Gamma_{(i,j)}$ is updated by the following:

$$\Gamma_{(i,j)}^+ = \sqrt{\frac{2v_{(i,j)}^+ \sigma_j(\bar{\mathcal{Y}}^{+(i)}) + v_{(i,j)}^2}{\Lambda_{(i,j)}^2}}. \quad (51)$$

Update \mathcal{X} : The closed form of \mathcal{X} can be derived by setting the derivative of (45) to zero. We can now update \mathcal{X} by the following equation:

$$\mathcal{X}^+ = \mathcal{P}_{\Omega^c} \left(\frac{\sum_{1 \leq l_1 < l_2 \leq N} \rho_{l_1 l_2} (\mathcal{Y}_{l_1 l_2} - \frac{Q_{l_1 l_2}}{\rho_{l_1 l_2}})}{\sum_{1 \leq l_1 < l_2 \leq N} \rho_{l_1 l_2}} \right) + \mathcal{P}_{\Omega}(\mathcal{Z}). \quad (52)$$

Update Q : Finally, multipliers $Q_{l_1 l_2}$ are updated as follows:

$$Q_{l_1 l_2}^+ = Q_{l_1 l_2} + \rho_{l_1 l_2} (\mathcal{X} - \mathcal{Y}_{l_1 l_2}). \quad (53)$$

The optimization steps of BEMCP formulation are listed in Algorithm 3. The main per-iteration cost lies in the update of $\mathcal{Y}_{l_1 l_2}$, which requires computing t-SVD. The per-iteration complexity is $O(LE(\sum_{1 \leq l_1 < l_2 \leq N} [\log(le_{l_1 l_2}) + \min(I_{l_1}, I_{l_2})]))$, where $LE = \prod_{i=1}^N I_i$ and $le_{l_1 l_2} = LE / (I_{l_1} I_{l_2})$.

VI. EXPERIMENTS

We evaluate the performance of the proposed LRTC methods. We employ the peak signal-to-noise rate (PSNR) value, the structural similarity (SSIM) value [40], the feature similarity (FSIM) value [41], and erreur relative globale adimensionnelle de synthèse (ERGAS) value [42] to measure the quality of the recovered results. The PSNR, SSIM, and FSIM

Algorithm 3 BEMCP

Input: An incomplete tensor \mathcal{Z} , the index set of the known elements Ω , convergence criteria ϵ , maximum iteration number K .

Initialization: $\mathcal{X}^0 = \mathcal{Z}_{\Omega}$, $\mathcal{Y}_{l_1 l_2}^0 = \mathcal{X}^0$, $\rho_{l_1 l_2}^0 > 0$, $\mu > 1$.

while not converged and $k < K$ **do**

Updating $\mathcal{Y}_{l_1 l_2}^k$ via (46);

Updating $W_{l_1 l_2}^k$ via (47);

Updating $\Lambda_{l_1 l_2}^k$ via (48);

Updating $\Gamma_{l_1 l_2}^k$ via (51);

Updating \mathcal{X}^k via (52);

Updating the multipliers $Q_{l_1 l_2}^k$ via (53);

$\rho_{l_1 l_2}^k = \mu \rho_{l_1 l_2}^{k-1}$, $k = k + 1$;

Check the convergence conditions $\|\mathcal{X}^{k+1} - \mathcal{X}^k\|_{\infty} \leq \epsilon$.

end while

return \mathcal{X}^{k+1} .

Output: Completed tensor $\mathcal{X} = \mathcal{X}^{k+1}$.

values are the bigger the better, and the ERGAS value is the smaller the better. All tests are implemented on the Windows 10 platform and MATLAB (R2019a) with an Intel Core i7-10875H 2.30 GHz and 32 GB of RAM.

In this section, we test three kinds of real-world data: MSI, MRI, and CV. The method for sampling the data is purely random sampling. The comparative LRTC methods are as follows: HaLRTC [43], LRTCCTV-I [44] represent state-of-the-art for the Tucker-decomposition-based methods; and TNN [45], PSTNN [46], FTNN [47], WSTNN [25] represent state-of-the-art for the t-SVD-based methods. Since the TNN, PSTNN, and FTNN methods only apply to three-order tensors, in all four-order tensor tests, we reshape them into three-order tensors and then test the performance of these methods.

A. MSI completion

We test 32 MSIs in the dataset CAVE¹. All testing data are of size $256 \times 256 \times 31$. In Fig.1, we randomly select three from 32 MSIs, bringing the different sampling rates and band visible results. The individual MSI names and their corresponding bands are written in the caption of Fig.1. As shown from Fig.1, the visual effect of the BEMCP is better than the contrast method at all three sampling rates. To further highlight the superiority of our method, the average quantitative results of 32 MSIs are listed in Table II. It can be seen that the three methods proposed in this paper have a great improvement compared to the WSTNN method. The PSNR value at both 10% and 20% sampling rate is at least 1.5dB higher than the WSTNN method, and even reaches 5dB at 5% sampling rate. Besides, the results show that the PSNR value of the BEMCP method is 0.2db higher than that of the EMCP method at all three sampling rates. This indicates that the BEMCP method is better than the univariate EMCP method. And compared with the NMCP method that directly uses the MCP function, our improvement is more prominent. More experimental results are available in Appendix A.

¹<http://www.cs.columbia.edu/CAVE/databases/multispectral/>

TABLE II
THE AVERAGE PSNR, SSIM, FSIM AND ERGAS VALUES FOR 32 MSIS TESTED BY OBSERVED AND THE NINE UTILIZED LRTC METHODS.

SR	5%				10%				20%				Time(s)
Method	PSNR	SSIM	FSIM	ERGAS	PSNR	SSIM	FSIM	ERGAS	PSNR	SSIM	FSIM	ERGAS	
Observed	15.438	0.153	0.644	845.339	15.673	0.194	0.646	822.808	16.185	0.269	0.651	775.716	0.000
HaLRTC	25.367	0.774	0.837	298.654	29.855	0.856	0.894	184.887	35.038	0.930	0.946	105.307	26.656
TNN	25.350	0.713	0.817	289.617	33.114	0.880	0.918	127.987	40.201	0.964	0.972	58.856	85.578
LRTCCTV-I	25.886	0.800	0.835	276.943	30.725	0.890	0.906	162.443	35.516	0.949	0.957	94.262	449.471
PSTNN	18.708	0.474	0.650	574.923	23.211	0.683	0.782	352.958	34.315	0.924	0.942	116.434	91.420
FTNN	32.645	0.899	0.924	131.419	37.151	0.954	0.963	78.977	43.023	0.984	0.987	41.714	503.684
WSTNN	31.431	0.806	0.911	208.954	40.143	0.981	0.981	53.010	47.049	0.995	0.995	24.974	125.812
NMCP	37.474	0.962	0.962	70.020	42.673	0.987	0.987	39.156	48.599	0.996	0.996	20.403	177.065
EMCP	37.602	0.960	0.961	69.286	43.507	0.987	0.987	35.883	49.668	0.995	0.996	17.996	194.907
BEMCP	37.939	0.963	0.963	66.775	43.734	0.988	0.988	34.998	49.904	0.996	0.996	17.551	204.299

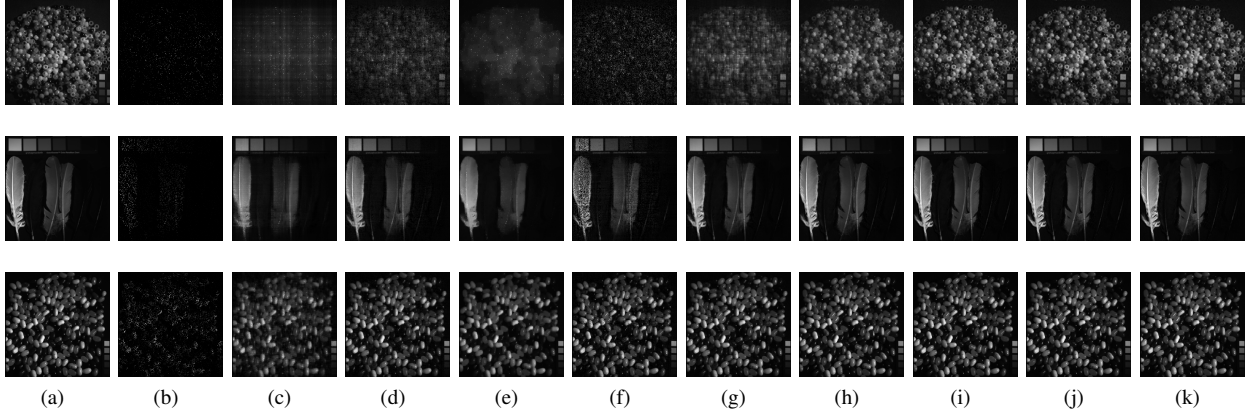


Fig. 1. (a) Original image. (b) Observed image. (c) HaLRTC. (d) TNN. (e) LRTCCTV-I. (f) PSTNN. (g) FTNN. (h) WSTNN. (i) NMCP. (j) EMCP. (k) BEMCP. SR: top row is 5%, middle row is 10% and last row is 20%. The rows of MSIs are in order: beads, feathers, jelly_beans. The corresponding bands in each row are: 31, 12, 20.

B. MRI completion

We test the performance of the proposed method and the comparative method on MRI² data with the size of $181 \times 217 \times 181$. First, we demonstrate the visual effect recovered by MRI data at sampling rates of 5%, 10% and 20% in Fig.2. Our method is clearly superior to the comparative methods. Then, we list the average quantitative results of frontal sections of MRI restored by all methods at different sampling rates in Table III. At the sampling rate of 5% and 10%, the PSNR value of the three methods is at least 1db higher than that of the WSTNN method. The PSNR value obtained by the BEMCP method is 0.4dB higher than that of the EMCP method at the sampling rate of 5% and 10%, and the values of SSIM, FSIM, and ERGAS are also better than the EMCP method.

C. CV completion

We test seven CVs³(respectively named news, akiyo, foreman, hall, highway, container, coastguard) of size $144 \times 176 \times 3 \times 50$. Firstly, we demonstrate the visual results of 7 CVs in our experiment in Fig.3, in which the number of frames and sampling rate corresponding to each CV are described in the caption of Fig.3. It is not hard to see from the picture that the recovery of our method on the vision effect is more better.

Furthermore, we list the average quantitative results of 7 CVs in Table IV. At this time, the suboptimal method is the EMCP. When the sampling rate is 5%, the PSNR value of our method is 0.5dB higher than it. In addition, at the sampling rate of 5% and 10%, the PSNR value of all three methods is at least 3db higher than that of the WSTNN method. More experimental results are available in Appendix B.

D. Discussions

1) *Model Analysis*: The two parameters α and ρ are included in our proposed BEMCP model. In addition, the initial values of the variables ν , Λ , and Γ also strongly influence on the efficient solution of the BEMCP model. The parameter values of α and ρ follow the settings in the N-tubal rank [25]. The initial value of the variable ν_0 is $\nu_0 = \Lambda_0 \star \Gamma_0$. The specific data affects the initial value design of Λ and Γ . The optimal initial value design can be found in Appendix C.

2) *Convergency Behaviours*: We take the LRTC of MSI, MRI, CV data as examples to illustrate the convergence behavior of the three algorithms under 5% sampling rate. We have drawn $\|\mathcal{X}^{k+1} - \mathcal{X}^k\|_\infty$ for each iteration in Fig.4. It can be seen that our algorithm converges stably and quickly.

VII. CONCLUSION

This paper proposes a new structural equivalence theorem called the BEMCP theorem, which converts two constant

²http://brainweb.bic.mni.mcgill.ca/brainweb/selection_normal.html

³<http://trace.eas.asu.edu/yuv/>

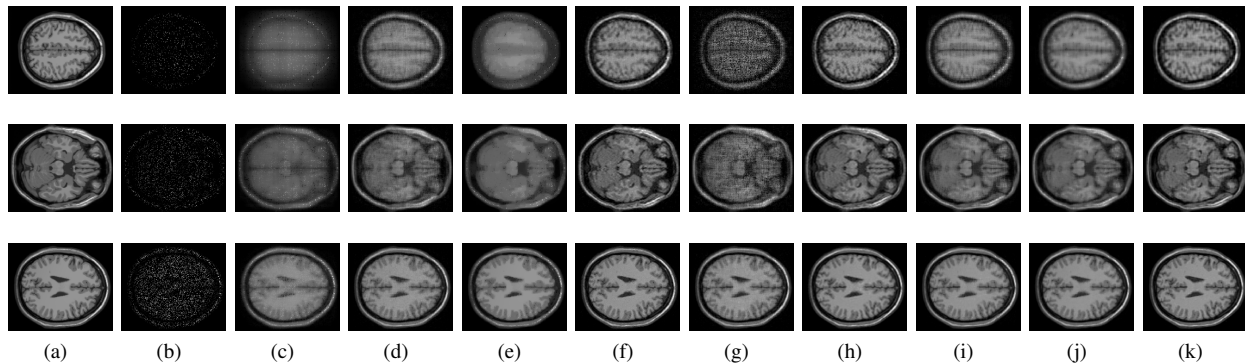


Fig. 2. (a) Original image. (b) Observed image. (c) HaLRTC. (d) TNN. (e) LRTCTV-I. (f) PSTNN. (g) FTNN. (h) WSTNN. (i) NMCP. (j) EMCP. (k) BEMCP. Each type of slice: the first row is the 120th slice with a sampling rate of 5%, the second row is the 50th slice with a sampling rate of 10%, and the third row is the 100th slice with a sampling rate of 20%.

TABLE III
THE PSNR, SSIM, FSIM AND ERGAS VALUES OUTPUT BY BY OBSERVED AND THE NINE UTILIZED LRTC METHODS FOR MRI.

SR	5%				10%				20%				Time(s)
	PSNR	SSIM	FSIM	ERGAS	PSNR	SSIM	FSIM	ERGAS	PSNR	SSIM	FSIM	ERGAS	
Observed	11.399	0.310	0.530	1021.050	11.634	0.323	0.565	993.910	12.147	0.350	0.613	936.861	0.000
HaLRTC	17.302	0.298	0.637	537.239	20.099	0.438	0.725	391.488	24.454	0.660	0.829	235.314	62.281
TNN	22.730	0.473	0.743	301.839	26.073	0.643	0.812	205.892	29.976	0.799	0.882	130.784	266.988
LRTCTV-I	19.369	0.597	0.702	433.001	22.824	0.749	0.805	295.265	28.202	0.890	0.908	155.596	1446.937
PSTNN	16.177	0.195	0.588	607.694	22.427	0.437	0.722	308.484	29.590	0.767	0.870	137.052	304.501
FTNN	24.881	0.694	0.836	231.536	28.324	0.826	0.895	152.216	32.690	0.923	0.945	90.268	3510.595
WSTNN	25.533	0.708	0.825	211.248	29.043	0.836	0.887	139.577	33.488	0.928	0.940	82.945	724.544
NMCP	28.874	0.814	0.871	140.651	32.338	0.902	0.919	94.670	35.822	0.952	0.954	62.815	821.349
EMCP	29.289	0.808	0.874	132.805	32.985	0.900	0.922	86.655	37.129	0.958	0.960	53.454	1061.362
BEMCP	29.734	0.834	0.883	126.610	33.392	0.912	0.928	82.986	37.194	0.960	0.961	53.102	1108.386

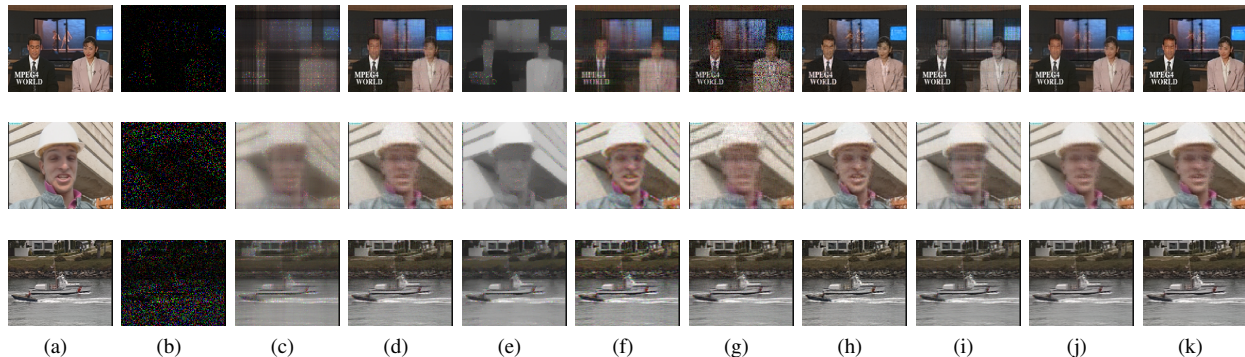


Fig. 3. (a) Original image. (b) Observed image. (c) HaLRTC. (d) TNN. (e) LRTCTV-I. (f) PSTNN. (g) FTNN. (h) WSTNN. (i) NMCP. (j) EMCP. (k) BEMCP. SR: top row is 5%, middle row is 10% and last row is 20%. The rows of CVs are in order: the 10th frame of news, the 30th frame of foreman, and the 45th frame of coastguard.

parameters in the MCP function into variables so that it can be adaptively updated with the iterative update of tensor singular values in the algorithm. Compared with other existing methods, the effect is remarkable, and it is slightly better than the same type of the NMCP and EMCP methods. On this basis, we give the BEMCP model for solving the LRTC problem. Extensive experiments show that our method can achieve better visual and numerical quantitative results than the comparison methods.

REFERENCES

- [1] Y.-M. Huang, H.-Y. Yan, Y.-W. Wen, and X. Yang, "Rank minimization with applications to image noise removal," *Information Sciences*, vol. 429, pp. 147–163, 2018.
- [2] B. Madathil and S. N. George, "Twist tensor total variation regularized-reweighted nuclear norm based tensor completion for video missing area recovery," *Information Sciences*, vol. 423, pp. 376–397, 2018.
- [3] Y. Wang, D. Meng, and M. Yuan, "Sparse recovery: from vectors to tensors," *National Science Review*, vol. 5, no. 5, pp. 756–767, 2018.
- [4] X.-L. Zhao, W.-H. Xu, T.-X. Jiang, Y. Wang, and M. K. Ng, "Deep plug-and-play prior for low-rank tensor completion," *Neurocomputing*, vol. 400, pp. 137–149, 2020.
- [5] S. Li, R. Dian, L. Fang, and J. M. Bioucas-Dias, "Fusing Hyperspectral and Multispectral Images via Coupled Sparse Tensor Factorization," *IEEE Transactions on Image Processing*, vol. 27, no. 8, pp. 4118–4130, 2018.
- [6] X. Fu, W.-K. Ma, J. M. Bioucas-Dias, and T.-H. Chan, "Semiblind Hyperspectral Unmixing in the Presence of Spectral Library Mismatches," *IEEE Transactions on Geoscience and Remote Sensing*, vol. 54, no. 9,

TABLE IV
THE AVERAGE PSNR, SSIM, FSIM AND ERGAS VALUES FOR 7 CVs TESTED BY OBSERVED AND THE NINE UTILIZED LRTC METHODS.

SR	5%				10%				20%				Time(s)
Method	PSNR	SSIM	FSIM	ERGAS	PSNR	SSIM	FSIM	ERGAS	PSNR	SSIM	FSIM	ERGAS	
Observed	5.793	0.011	0.420	1194.940	6.028	0.019	0.423	1163.038	6.540	0.034	0.429	1096.477	0.000
HaLRTC	17.336	0.488	0.695	329.173	21.141	0.622	0.774	214.642	24.981	0.772	0.862	137.634	13.980
TNN	27.033	0.771	0.886	113.454	30.453	0.855	0.928	79.511	33.697	0.910	0.955	56.639	44.979
LRTCTV-I	19.497	0.579	0.692	272.767	21.205	0.655	0.771	228.491	25.812	0.817	0.881	126.740	281.989
PSTNN	16.151	0.312	0.664	364.981	27.897	0.778	0.890	102.835	33.258	0.906	0.952	58.772	44.823
FTNN	25.286	0.766	0.871	137.494	28.544	0.858	0.917	93.393	32.214	0.924	0.954	61.414	373.005
WSTNN	29.257	0.872	0.920	88.184	32.635	0.924	0.952	62.072	36.557	0.960	0.975	40.820	197.168
NMCP	30.432	0.885	0.933	77.007	33.934	0.933	0.961	52.983	37.399	0.963	0.980	35.450	211.281
EMCP	30.768	0.887	0.937	74.465	34.512	0.934	0.964	50.102	38.204	0.964	0.982	32.499	226.812
BEMCP	31.284	0.893	0.942	70.978	34.683	0.935	0.965	49.164	38.244	0.964	0.982	32.285	247.195

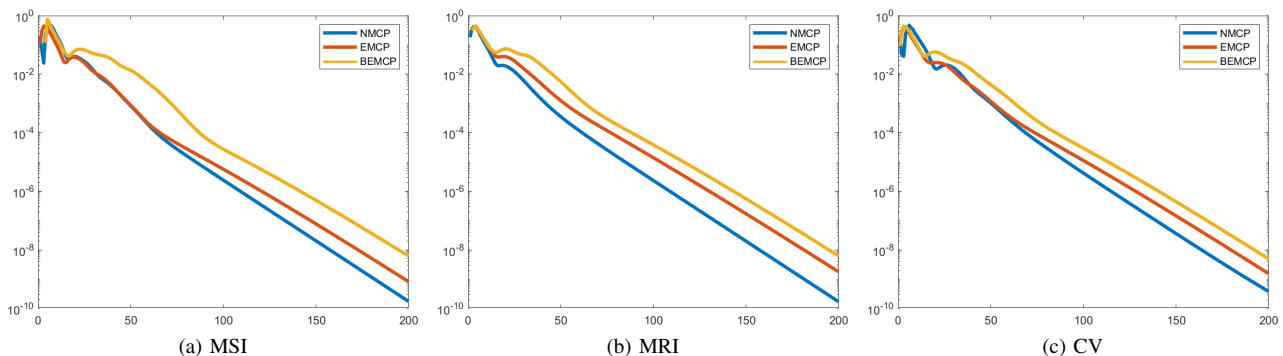


Fig. 4. The convergence behaviours of LRTC algorithm, with respect to MSI, MRI, CV data.

- pp. 5171–5184, 2016.
- [7] J. Xue, Y. Zhao, W. Liao, and J. C.-W. Chan, “Nonlocal Low-Rank Regularized Tensor Decomposition for Hyperspectral Image Denoising,” *IEEE Transactions on Geoscience and Remote Sensing*, vol. 57, no. 7, pp. 5174–5189, 2019.
- [8] J. Xue, Y. Zhao, W. Liao, J. C.-W. Chan, and S. G. Kong, “Enhanced Sparsity Prior Model for Low-Rank Tensor Completion,” *IEEE Transactions on Neural Networks and Learning Systems*, vol. 31, no. 11, pp. 4567–4581, 2020.
- [9] J.-H. Yang, X.-L. Zhao, T.-Y. Ji, T.-H. Ma, and T.-Z. Huang, “Low-rank tensor train for tensor robust principal component analysis,” *Applied Mathematics and Computation*, vol. 367, p. 124783, 2020.
- [10] T.-X. Jiang, T.-Z. Huang, X.-L. Zhao, T.-Y. Ji, and L.-J. Deng, “Matrix factorization for low-rank tensor completion using framelet prior,” *Information Sciences*, vol. 436, pp. 403–417, 2018.
- [11] M. Ding, T.-Z. Huang, T.-Y. Ji, X.-L. Zhao, and J.-H. Yang, “Low-rank tensor completion using matrix factorization based on tensor train rank and total variation,” *Journal of Scientific Computing*, vol. 81, no. 2, pp. 941–964, 2019.
- [12] J. Xue, Y. Zhao, W. Liao, and J. Cheung-Wai Chan, “Nonconvex tensor rank minimization and its applications to tensor recovery,” *Information Sciences*, vol. 503, pp. 109–128, 2019.
- [13] I. Kajo, N. Kamel, Y. Ruichek, and A. S. Malik, “SVD-Based Tensor-Completion Technique for Background Initialization,” *IEEE Transactions on Image Processing*, vol. 27, no. 6, pp. 3114–3126, 2018.
- [14] W. Cao, Y. Wang, J. Sun, D. Meng, C. Yang, A. Cichocki, and Z. Xu, “Total Variation Regularized Tensor RPCA for Background Subtraction From Compressive Measurements,” *IEEE Transactions on Image Processing*, vol. 25, no. 9, pp. 4075–4090, 2016.
- [15] W. Wei, L. Yi, Q. Xie, Q. Zhao, D. Meng, and Z. Xu, “Should We Encode Rain Streaks in Video as Deterministic or Stochastic?” in *2017 IEEE International Conference on Computer Vision (ICCV)*, 2017, pp. 2535–2544.
- [16] M. Li, Q. Xie, Q. Zhao, W. Wei, S. Gu, J. Tao, and D. Meng, “Video Rain Streak Removal by Multiscale Convolutional Sparse Coding,” in *2018 IEEE/CVF Conference on Computer Vision and Pattern Recognition*, 2018, pp. 6644–6653.
- [17] Q. Zhao, L. Zhang, and A. Cichocki, “Bayesian CP Factorization of Incomplete Tensors with Automatic Rank Determination,” *IEEE Transactions on Pattern Analysis and Machine Intelligence*, vol. 37, no. 9, pp. 1751–1763, 2015.
- [18] T. Yokota, N. Lee, and A. Cichocki, “Robust Multilinear Tensor Rank Estimation Using Higher Order Singular Value Decomposition and Information Criteria,” *IEEE Transactions on Signal Processing*, vol. 65, no. 5, pp. 1196–1206, 2017.
- [19] E. Acar, D. M. Dunlavy, T. G. Kolda, and M. Mørup, “Scalable tensor factorizations for incomplete data,” *Chemometrics and Intelligent Laboratory Systems*, vol. 106, no. 1, pp. 41–56, 2011.
- [20] P. Tichavský, A.-H. Phan, and A. Cichocki, “Numerical CP decomposition of some difficult tensors,” *Journal of Computational and Applied Mathematics*, vol. 317, pp. 362–370, 2017.
- [21] Y.-F. Li, K. Shang, and Z.-H. Huang, “Low Tucker rank tensor recovery via ADMM based on exact and inexact iteratively reweighted algorithms,” *Journal of Computational and Applied Mathematics*, vol. 331, pp. 64–81, 2018.
- [22] X. Li, M. K. Ng, G. Cong, Y. Ye, and Q. Wu, “MR-NTD: Manifold Regularization Nonnegative Tucker Decomposition for Tensor Data Dimension Reduction and Representation,” *IEEE Transactions on Neural Networks and Learning Systems*, vol. 28, no. 8, pp. 1787–1800, 2017.
- [23] Z. Zhang, G. Ely, S. Aeron, N. Hao, and M. Kilmer, “Novel Methods for Multilinear Data Completion and De-noising Based on Tensor-SVD,” *2014 IEEE Conference on Computer Vision and Pattern Recognition*, pp. 3842–3849, 2014.
- [24] C. J. Hillar and L.-H. Lim, “Most tensor problems are NP-hard,” *Journal of the ACM (JACM)*, vol. 60, no. 6, pp. 1–39, 2013.
- [25] Y.-B. Zheng, T.-Z. Huang, X.-L. Zhao, T.-X. Jiang, T.-Y. Ji, and T.-H. Ma, “Tensor N-tubal rank and its convex relaxation for low-rank tensor recovery,” *Information Sciences*, vol. 532, pp. 170–189, 2020.
- [26] I. Selesnick, “Sparse regularization via convex analysis,” *IEEE Transactions on Signal Processing*, vol. 65, no. 17, pp. 4481–4494, 2017.
- [27] B. K. Natarajan, “Sparse approximate solutions to linear systems,” *SIAM Journal on Computing*, vol. 24, no. 2, pp. 227–234, 1995.
- [28] Y. Hu, D. Zhang, J. Ye, X. Li, and X. He, “Fast and Accurate Matrix Completion via Truncated Nuclear Norm Regularization,” *IEEE Transactions on Pattern Analysis and Machine Intelligence*, vol. 35, no. 9, pp. 2117–2130, 2013.
- [29] B. Recht, M. Fazel, and P. A. Parrilo, “Guaranteed minimum-rank

- solutions of linear matrix equations via nuclear norm minimization,” *SIAM Review*, vol. 52, no. 3, pp. 471–501, 2010.
- [30] D. Qiu, M. Bai, M. K. Ng, and X. Zhang, “Nonlocal robust tensor recovery with nonconvex regularization,” *Inverse Problems*, vol. 37, no. 3, p. 035001, 2021.
- [31] C. Lu, C. Zhu, C. Xu, S. Yan, and Z. Lin, “Generalized singular value thresholding,” *Proceedings of the AAAI Conference on Artificial Intelligence*, vol. 29, no. 1, 2015.
- [32] C.-H. Zhang, “Nearly unbiased variable selection under minimax concave penalty,” *The Annals of statistics*, vol. 38, no. 2, pp. 894–942, 2010.
- [33] P. K. Pokala, R. V. Hemadri, and C. S. Seelamantula, “Iteratively Reweighted Minimax-Concave Penalty Minimization for Accurate Low-rank Plus Sparse Matrix Decomposition,” *IEEE Transactions on Pattern Analysis and Machine Intelligence*, 2021.
- [34] S. Boyd, N. Parikh, and E. Chu, *Distributed optimization and statistical learning via the alternating direction method of multipliers*. Now Publishers Inc, 2011.
- [35] Z. Lin, R. Liu, and Z. Su, “Linearized Alternating Direction Method with Adaptive Penalty for Low-Rank Representation,” *Advances in Neural Information Processing Systems*, vol. 24, pp. 612–620, 2011.
- [36] M. E. Kilmer and C. D. Martin, “Factorization strategies for third-order tensors,” *Linear Algebra and its Applications*, vol. 435, no. 3, pp. 641–658, 2011.
- [37] C. Lu, J. Feng, Y. Chen, W. Liu, Z. Lin, and S. Yan, “Tensor Robust Principal Component Analysis with a New Tensor Nuclear Norm,” *IEEE Transactions on Pattern Analysis and Machine Intelligence*, vol. 42, no. 4, pp. 925–938, 2020.
- [38] L. Mirsky, “A trace inequality of John von Neumann,” *Monatshefte für mathematik*, vol. 79, no. 4, pp. 303–306, 1975.
- [39] Z. Lin, M. Chen, and Y. Ma, “The augmented lagrange multiplier method for exact recovery of corrupted low-rank matrices,” *arXiv preprint arXiv:1009.5055*, 2010.
- [40] Z. Wang, A. Bovik, H. Sheikh, and E. Simoncelli, “Image quality assessment: from error visibility to structural similarity,” *IEEE Transactions on Image Processing*, vol. 13, no. 4, pp. 600–612, 2004.
- [41] L. Zhang, L. Zhang, X. Mou, and D. Zhang, “FSIM: A Feature Similarity Index for Image Quality Assessment,” *IEEE Transactions on Image Processing*, vol. 20, no. 8, pp. 2378–2386, 2011.
- [42] L. Wald, *Data fusion: definitions and architectures: fusion of images of different spatial resolutions*. Presses des MINES, 2002.
- [43] J. Liu, P. Musialski, P. Wonka, and J. Ye, “Tensor Completion for Estimating Missing Values in Visual Data,” *IEEE Transactions on Pattern Analysis and Machine Intelligence*, vol. 35, no. 1, pp. 208–220, 2013.
- [44] X. Li, Y. Ye, and X. Xu, “Low-rank tensor completion with total variation for visual data inpainting,” *Proceedings of the AAAI Conference on Artificial Intelligence*, vol. 31, no. 1, 2017.
- [45] Z. Zhang and S. Aeron, “Exact Tensor Completion Using t-SVD,” *IEEE Transactions on Signal Processing*, vol. 65, no. 6, pp. 1511–1526, 2017.
- [46] T.-X. Jiang, T.-Z. Huang, X.-L. Zhao, and L.-J. Deng, “Multi-dimensional imaging data recovery via minimizing the partial sum of tubal nuclear norm,” *Journal of Computational and Applied Mathematics*, vol. 372, p. 112680, 2020.
- [47] T.-X. Jiang, M. K. Ng, X.-L. Zhao, and T.-Z. Huang, “Framelet Representation of Tensor Nuclear Norm for Third-Order Tensor Completion,” *IEEE Transactions on Image Processing*, vol. 29, pp. 7233–7244, 2020.